General Disclaimer

One or more of the Following Statements may affect this Document

- This document has been reproduced from the best copy furnished by the organizational source. It is being released in the interest of making available as much information as possible.

- This document may contain data, which exceeds the sheet parameters. It was furnished in this condition by the organizational source and is the best copy available.

- This document may contain tone-on-tone or color graphs, charts and/or pictures, which have been reproduced in black and white.

- This document is paginated as submitted by the original source.

- Portions of this document are not fully legible due to the historical nature of some of the material. However, it is the best reproduction available from the original submission.

Experimental Evaluation of Cascade

D. E. Boldman, A. R. Bloomer, and E. M. Shaw
Lewis Research Center
Cleveland, Ohio

Prepared for the
Twenty-First Aerospace Sciences Conference
sponsored by the American Institute of
Aeronautics and Astronautics
Reno, Nevada, January 10-13, 1983

NASA

EXPERIMENTAL EVALUATION OF SHOCKLESS SUPERCRITICAL AIRFOILS IN CASCADE

D. R. Boldman,* A. E. Buggele,** and L. M. Shaw**
National Aeronautics and Space Administration
Lewis Research Center
Cleveland, OH 44135

Abstract

Surface Mach number distributions, total pressure loss coefficients, and schlieren images of the flow are presented over a range of inlet Mach numbers and air angles. Several different trailing edge geometries were tested. At design conditions a leading edge separation bubble was observed resulting in higher losses than anticipated. The minimum losses were obtained at a negative incidence condition in which the flow was accelerating over most of the supercritical region. Relatively minor differences in losses were measured with the different trailing edge geometries studied.

Nomenclature

AVDR	axial velocity density ratio, $\rho_2 V_{x2}/\rho_1 V_{x1}$
c	airfoil chord
M	Mach number
P	pressure
Re_c	Reynolds number based on chord
s	arc length
SP	separation parameter, $-\theta dV_e/V_e ds$
V	velocity
X,Y	rectangular coordinates
β_1	inlet air angle relative to X-axis
$\Delta\beta_1$	difference between actual and design air angles, $\beta_1 - \beta_{1des}$
γ	stagger angle (see Fig. 2)
θ	boundary layer momentum thickness
i	incidence angle (see Fig. 2)
ρ	density
τ	airfoil gap (see Fig. 2)
ω	total pressure loss coefficient, $(P_{t1} - \langle P_{t2}\rangle)/(P_{t1} - P_1)$
<>	mass-averaged quantity
Subscripts	
1	inlet conditions
2	exit conditions
des	design condition
e	edge of boundary layer
t	total condition
x	axial direction

I. Introduction

The application of supercritical wing theory to the design of blades for turbomachinery is attractive because of the potential for improved efficiency and increased flow range at low loss resulting from a shock-free flow field. Studies of two-dimensional supercritical airfoils in cascade constitute an important step in the verification of design theory and improving our overall understanding of "shockless" transonic flow in turbomachinery. The present investigation represents such a study whereby the experimental performance of a linear cascade of two-dimensional supercritical airfoils was determined for a range of inlet air angles and Mach numbers.

An important aspect of this study was the utilization of a schlieren system for flow visualization to determine whether the cascaded airfoils were operating free of shocks in accordance with theory. Strong evidence of shockless operation in a linear cascade has been provided by Stephens[1] and Rechter et.al[2] on the basis of observed Mach number distributions in conjunction with good agreement between the experiment and supercritical cascade theory. In the present investigation, schlieren photographs are used to supplement the observed Mach number distributions and total pressure loss coefficients in order to provide visual evidence of the quality of the shock-free flow field associated with cascaded supercritical airfoils.

The experiment was performed in the linear transonic cascade facility described by Boldman et.al.[3] The cascade tunnel was originally designed for transonic flutter experiments with low turning, highly staggered rotor type airfoils but was modified for the present study in order to accommodate airfoils with high turning, low stagger angles. Such airfoils are representative of compressor stator blades.

The airfoils used in this program were scaled up from the coordinates for the mean section of a supercritical compressor stator blade having approximately 35° of turning. The airfoils were designed by the method of Bauer, Garabedian, and Korn[4] (BGK) whereby the pressure distribution on the airfoil surface is prescribed as part of the input. This general design procedure, often referred to as an inverse method, has become recognized because it can be used to generate airfoils with high loading but without strong shocks and the attendant losses.

Acknowledgements

The authors wish to thank Dr. Jose Sanz and Mr. James Schmidt for performing the design and analysis computations. The authors are also grateful to Mr. Thomas Gelder for his guidance and many helpful suggestions concerning the experiment.

II. Design Considerations

The general design procedure, which involved the method of complex characteristics and hodograph transformation, has been well documented[4,5] therefore only key elements of the method will be presented herein. The airfoils were designed to meet specific inlet and exit flow conditions for the stator row of a single-stage axial flow compressor. In order to meet these boundary conditions, 35° of turning were required. An initial surface Mach number distribution was prescribed and the two-dimensional potential flow equations were solved to generate an airfoil geometry consistent with the boundary conditions. Viscous effects were then introduced into the procedure to account for the displacement thickness of the boundary layer.

In the boundary layer calculations used with the BGK design method, the laminar layer is ignored and a turbulent layer is calculated starting from designated locations on the suction and pressure surfaces. These locations were determined for the present design with an integral boundary layer calculation by McNally.[6] A laminar boundary layer was calculated starting from the leading edge until transition or separation was indicated. For the

*Research Engineer, Associate Fellow
**Research Engineer, Member, AIAA

present study, separation was indicated before transition at 35-percent chord on the suction surface and at 11-percent chord on the pressure surface. Starting from these locations, the turbulent boundary layer calculation to the trailing edge was made within the BGK design code using the integral method of Nash-Macdonald.(7) To start the turbulent boundary layer calculation used with the BGK method, an initial boundary layer momentum thickness Reynolds number of 320 was assumed. This equals the minimum value experimentally observed for a turbulent layer by Preston.(8) A Stratford(9) separation parameter, SP, is used in the Nash-Macdonald method to indicate turbulent boundary layer separation. This separation parameter is defined as

$$SP = -\frac{\theta}{V_e}\frac{dV_e}{ds}$$

with the critical value for separation of 0.004. The maximum value of SP allowed in the present designs was a conservative value of about 0.003. The inviscid and viscous flow analyses were repeated until an acceptable airfoil shape was attained within this limit.

Two basic airfoil geometries were studied in the present experiment. The airfoils were designed for different Reynolds numbers based on chord but with all other conditions fixed. Consequently, the only difference in calculated airfoil geometry was the result of the influence of Reynolds number on the turbulent boundary layer calculation. The first airfoil was designed for a Reynolds number of 0.7×10^6 corresponding to the value in a single-stage compressor facility. This resulted in an airfoil with a relatively thick trailing edge of 3.9-percent chord. The second airfoil was designed for a Reynolds number of 1.4×10^6 corresponding to the nominal level in which the cascade experiments were performed. This resulted in an airfoil with a relatively thin trailing edge of 1.64-percent chord. The difference in airfoil geometry in the region from the start of the turbulent boundary layer calculations to the trailing edge is due to the smaller initial thickness of the boundary layer for the higher Reynolds number airfoil. This follows from the previous discussion and the relation

$$\frac{\theta}{C} \approx \frac{320}{Re_C}$$

The initially thinner boundary layer is able to negotiate more diffusion with the same value of the separation parameter than the initially thicker layer. The end result is a thinner airfoil as the trailing edge is approached.

Both airfoils were tested in cascade but only at the higher Reynolds number of 1.4×10^6. A limited number of tests were also performed with rounded and squared trailing edges to assess the effect of trailing edge shape on the performance. The airfoils and the design surface Mach number distribution are shown in Figure 1 for the thick trailing edge airfoil. This distribution is essentially representative of the design for the thin trailing edge airfoil as well. Also shown are the starting locations of the turbulent boundary layers on each surface as previously discussed.

The design code based on the BGK method could not be used for off-design calculations. At off-design conditions the calculations were performed using the inviscid analysis code QSONIC.(10) The results from the BGK and QSONIC codes are compared in Figure 1 at design conditions. Slight differences in the suction surface Mach number distributions are apparent near the 30 percent chord region; however over the remainder of the airfoil the agreement between the two methods is good.

The coordinate system and design conditions are summarized in Fig. 2. All angles are measured relative to the X-axis. In the presentation of the results, the inlet air angle will be given as a difference $\Delta\beta_1$ where

$$\Delta\beta_1 = \beta_1 - \beta_{1des}$$

III. Cascade Facility and Instrumentation

The experimental program was performed in a transonic linear cascade facility which was originally designed for flutter experiments. This cascade was reconfigured for the present experiments as shown schematically in Fig. 3. In the original flutter cascade, the inlet boundary layer was removed with a suction system containing flush-mounted perforated plates approximately one chord length upstream of the airfoils. It was recognized that this system alone would probably be inadequate for the present program because the supercritical airfoils had much greater turning and a lower aspect ratio than the airfoils used in the flutter studies. Therefore two other independent suction systems were added.

The first of these systems consisted of 0.32 cm wide by 5.6 cm long corner slots (Peacock(11)) which extended over the downstream half of the suction surface of each airfoil. The other system contained perforated plates between the airfoils to supplement flow removal by the corner slots. These two suction systems were separated by partitions as shown in Fig. 4(a). Experience revealed that the perforated plate, which originally encompassed the full blade-to-blade gap, introduced undesirable disturbances which influenced the wake measurements. After a number of iterations it was learned that a triangular passage shape in conjunction with the corner slots produced the best end wall boundary layer control based on wake measurements from the combination probe. The triangular passage, shown in Fig. 4(a), was obtained by applying metallic tape over a portion of the perforated suction flow passage. Ambient air was drawn through the cascade by a continuous-flow exhaust system operating at a nominal pressure of 27.6 kPa.

The free stream turbulence level approximately 1.5 chord lengths upstream of the leading edge of the blade row was nominally 0.6 percent at Mach numbers up to 0.4. Turbulence measurements were not made at higher Mach numbers because of the complications associated with compressibility effects; however the turbulence intensity at higher Mach numbers is expected to be about the same. Flow rates were controlled by two downstream throttle valves. All of the suction systems for boundary layer control were also coupled to this exhaust system through a series of independent manifolds and valves.

The cascade had an airfoil gap τ of 11.7 cm which was fixed by the existing end walls. This gap, in conjunction with the required design solidity (C/τ) of 0.91, yieldeo a chord of 10.7 cm. With this chord and an end wall spacing of 9.7 cm, the airfoil aspect ratio (span to chord) was 0.91.

In the flow visualization phase of the experiment, the back perforated end wall in the central

passage of the cascade was replaced with a 0.64-cm-thick mirror as shown in Fig. 4(b). An optical quality glass window was installed in the other end wall. The mirror and window contained the corner slot for boundary layer suction; however, the triangular passage could not be used. This did not seriously compromise the flow visualization study because the corner slots produced the most effective mechanism for end wall boundary control. The window and mirror arrangement constituted part of a double-pass schlieren system which is shown schematically in Fig. 5. Images of the flow field were recorded on 70 mm film while operating the light source in a pulsed mode.

Pressures from rows of wall static taps upstream and downstream of the cascade were monitored as part of the procedure to establish periodicity in the cascade. The pressure taps were spaced 2.92 cm apart in the tangential direction (25 percent of the blade spacing). The rows of taps were located 0.13 and 0.34 chord lengths in the axial direction upstream and downstream of the airfoils, respectively.

Static pressures were measured at 15 positions on the suction surface of one airfoil and at 10 positions on the pressure surface of another airfoil. These two airfoils were arranged so that the pressures corresponding to the flow in the central blade passage were measured.

Additional static pressure taps were included in all of the boundary layer bleed passages, the tailboards, and the side walls. These pressures were monitored as part of the procedure to establish periodicity in the cascade.

A combination probe was located one-half chord length downstream of the cascade as shown in Fig. 3. This probe measured the local values of total and static pressure as well as a differential pressure related to the flow angle as it was traversed in the tangential direction. These measurements were used to establish periodicity on the basis of blade-to-blade wake consistency at the centerline of the flow channel. The local values of total and static pressure were used to calculate the local Mach number. These local quantities were mass-averaged over the central passage to give the exit Mach number, total pressure, and flow angle. Other exit parameters such as the axial velocity density ratio (AVDR) were computed from these mass-averaged primary variables.

The total instrumentation system included over 200 channels of pressures and temperatures which were recorded with a system of micro-processors coupled to a dedicated mini-computer. Most of the pressures including end wall and airfoil static pressures were connected to a scanivalve system containing four 48-channel units scanning in parallel at a rate of 7 samples per second. The remainder of the pressures, including reference values for the scanivalve system and pressures from the downstream combination probe, were recorded through a system of signal conditioners and pressure transducers. Research and graphic CRT displays were used to expedite tuning of the cascade and provide on-line performance data. An X-Y plotter was used to monitor the output from the exit combination probe during the tuning process. Upon completion of the tuning, the combination probe was traversed in a stepwise mode over one blade gap in the center of the cascade to provide the exit flow conditions. Detailed flow calculations were performed with an IBM 370 computer which provided on-line performance data from the pressures on the airfoil and combination probe.

IV. Test Procedure

Special procedures were required in order to determine the inlet Mach number and flow angle. Both of these quantities were based on measurements obtained 0.13 to 0.15 chord lengths upstream of the cascade. The flow field is highly non-uniform in this region because of the close proximity to the airfoils; therefore it was necessary to determine the inlet conditions by an indirect method involving the experimental pressure measurements in combination with the calculated potential flow field. In this procedure, the inlet Mach number was based on the inlet total pressure and an average of five wall static pressures across the central blade passage whereas the flow angle was determined from the average angle provided by three null-type flow angle probes.

The inlet air angle did not generally coincide with the setting angle of the hinged inlet walls. The upstream end wall bleed system had a strong influence on the inlet air angle causing differences of up to 5° between inlet setting angle and air angle. Therefore it was difficult to determine, apriori, the inlet flow angle on the basis of the inlet setting angle. In order to approach the design and minimum loss conditions, data were obtained for a number of inlet setting angles with the actual flow angle determined from the flow angle probes. In this way, the exact design value of inlet air angle ($\Delta\beta_1 = 0$) was not obtained; however a value of $\Delta\beta_1$ very close to design was achieved (i.e., $\Delta\beta_1 = -0.4°$). Details of the method of determining the inlet Mach number and air angle are presented in the Appendix.

V. Results and Discussion

In the following presentation of surface Mach number distributions, the values of AVDR and total pressure loss coefficient ω will be given in the figures. AVDR, which is a measure of the flow blockage across cascaded airfoils, can be expressed as

$$\text{AVDR} = \frac{\rho_2 V_{x2}}{\rho_1 V_{x1}}$$

A number of investigators[12-14] have indicated the importance of AVDR in interpreting cascade data. Since AVDR is based on simple continuity considerations, it includes the effects of physical blockage due to such things as contracting end walls and/or thick trailing edge airfoils as well as the displacement effect of the boundary layer on these surfaces. The value of AVDR would be unity for a two-dimensional inviscid flow over airfoils having sharp trailing edges. For two-dimensional inviscid flow over thick trailing edge airfoils the AVDR would be slightly greater than unity as a result of the blockage imposed by the thickness of the trailing edge. AVDR can be controlled by varying the end wall suction in the cascade; however in the present study it was more practical to optimize the suction at the design Mach number and perform the off-design tests without altering the suction valve settings. The optimum suction condition was established on the basis of blade-to-blade wake consistency combined with wake minimum pressure loss as determined from X-Y plots of the pressure from the combination probe. The values of AVDR, which were determined from the combination probe measurements, varied from about 1.03 to 1.09 over the Mach number range of 0.7 to 0.8.

A measure of the performance of the cascade is given by the total pressure loss coefficient, ω, where

$$\omega = \frac{P_{t1} - \langle P_{t2} \rangle}{P_{t1} - P_1}$$

The mass-averaged value $\langle P_{t2} \rangle$ in this equation was obtained from the combination probe located at the centerline of the cascade. This probe traversed over the central blade passage at a distance of one-half chord length downstream of the trailing edge of the airfoils.

Surface Mach Numbers and Loss Coefficients Near Design Conditions. The experimental Mach number distributions are presented for the thin trailing edge airfoil operating at both the near-design inlet air angle ($\Delta\beta_1 = -0.4^\circ$) and at the minimum loss angle ($\Delta\beta_1 = -2.5^\circ$) for inlet Mach numbers of 0.70, 0.75, and 0.80 in Figs. 6 and 7, respectively. A region of supersonic flow extends from about the 5 percent chord point to the 50 percent chord point for all of these inlet Mach numbers. The results for the suction surface at $\Delta\beta_1 = -0.4^\circ$ (Fig. 6(a)) do not reveal the flat distribution of Mach number in the supersonic region that would be expected on the basis of the BGK design theory. This behavior was attributed to the presence of a long laminar separation bubble commencing near the 10 percent chord location. This was confirmed by observing the surface flow patterns as alcohol was injected into the static pressure taps. This separation bubble persisted despite attempts to eliminate it by varying the relative amounts of boundary layer suction upstream and within the blade passage.

When the inlet air angle was changed to provide a more negative incidence angle ($\Delta\beta_1 = -2.5^\circ$), the flow tended to accelerate in much of the supersonic region and the presence of the strong separation bubble was not as apparent. This is especially evident in the profile for $M_1 = 0.75$, shown in Fig. 7(a). Also the total pressure loss coefficient at this condition was lower than the corresponding value at $\Delta\beta_1 = -0.4^\circ$ (Fig. 6(a)) where early separation was observed on the suction surface.

Mach number distributions corresponding to airfoils with thick and thin trailing edges are shown in Fig. 8 for the design value of inlet Mach number and the minimum-loss inlet air angle. Although some differences in the data are apparent, the basic features which were described previously are evident. The data presented in Fig. 8(a) were obtained by first testing the thick trailing edge airfoil throughout the range of parameters. The thin airfoil cascade was then installed and the tests were performed in a similar manner.

The differences in the Mach number distributions shown in Fig. 8(a) are attributed to a sensitivity of the flow to small differences in air angle and suction flow resulting from independent tests of the two cascades. In order to minimize these types of errors, the experiment was rerun by first testing the thin trailing edge airfoil at a fixed suction flow and geometric arrangement and then repeating the tests with the thick trailing edge airfoil. In this latter case the thick trailing edge was formed by adding a contoured wedge section of balsa to the thin airfoils while fixed in position in the cascade. The results shown in Fig. 8(b) reveal that the trailing edge thickness indeed had a negligible influence on the Mach number distributions. This was also observed at the near-design inlet air angle of $\Delta\beta_1 = -0.4^\circ$.

The total pressure loss coefficient was only slightly higher with the thick trailing edge airfoils. The loss coefficient for the thick trailing edge airfoil was nominally 0.049 compared to a value of 0.040 for the thin trailing edge airfoil as indicated in Fig. 8.

Another aspect of this study concerned the effect of trailing edge geometry on the performance. The original airfoil, which had a squared trailing edge, was modified by adding a round trailing edge of balsa. The results for these two trailing edge geometries, shown in Fig. 9, reveal only a small influence of the trailing edge shape on the suction surface Mach number distributions and a slightly higher total pressure loss coefficient with the round trailing edge configuration. Similar results were obtained with the thin trailing edge airfoils.

Loss Coefficients over a Range of Inlet Mach Numbers and Air Angles. Total pressure loss coefficients for the thin trailing edge airfoil are presented as a function of inlet air angle and inlet Mach number in Fig. 10. The minimum loss condition at the design inlet Mach number occurred at an air angle of about -2.5°. The minimum loss point shifts slightly to more positive incidence angles as the inlet Mach number increases. Minimum losses at the design Mach number were about 0.04. Slightly higher loss coefficients were obtained with the thick trailing edge airfoil as noted by the shaded symbols in Fig. 10.

The loss coefficients at the minimum loss inlet air angle are plotted as a function of Mach number in Fig. 11. The lowest losses were obtained with the thin trailing edge airfoil. Slightly higher losses accompanied the thick rounded edge airfoil relative to the squared edge airfoil; however the differences over most of the Mach number range are small.

Flow Visualization. In order to use the schlieren system only the corner slot suction system was retained as shown in Fig. 4(b). The Mach number distribution with only the slot suction system (and schlieren system) was essentially the same as the results obtained with the full suction system as shown in Fig. 12. It is believed that the good agreement exists because in the full suction system most of the end wall flow was removed by the corner slots. Excessive flow through the perforated passage bleed adversely affected the wake measurements by introducing what appeared to be secondary flow. Consequently, very little flow was removed from the perforated plate passages. The observed sensitivity of the wake behavior to the amount of passage bleed flow is believed to be related to the small aspect ratio of the cascade.

Schlieren photographs of the flow over the thin trailing edge airfoil are shown in Fig. 13. The first series of schlieren images (Figs. 13(a) to (d)) were obtained at various inlet Mach numbers for the minimum loss inlet air angle of -2.5°. Figure 13(e) shows the flow field at the design Mach number and the near-design inlet air angle of -0.4° corresponding to the conditions in which a laminar separation bubble was observed near the leading edge.

Figures 13(a) ($M_1 = 0.70$) and 13(b) ($M_1 = 0.73$) show weak shocks near midchord and no evidence of boundary layer separation on the suction surface. Low loss levels, which would be expected at these conditions, were indeed obtained as shown in Figure 11 where $\omega = 0.024$ and 0.032 for $M_1 = 0.70$ and 0.73, respectively. Also there was no evidence of

separation based on the surface Mach number distributions shown in Fig. 7.

In Figure 13(c) (M_1 = 0.75) the shocks near midchord are not much different from those shown in Figs. 13(a) and (b), but at this slightly higher Mach number there is a definite indication that the boundary layer separates just downstream of the shock. In Figure 13(d) (M_1 = 0.80) a more extensive and probably stronger shock array is evident resulting in a somewhat thicker separated region. As expected, the losses at these Mach numbers are higher: ω = 0.04 and 0.10 for M_1 = 0.75 and 0.80, respectively. The large differences in these losses is not apparent from the schlieren images alone. However the surface Mach number distributions in Fig. 7 suggest an appreciable increase in loss for the case in which M_1 = 0.80 relative to that for M_1 = 0.75 because of the early flattening of the surface Mach numbers near 60-percent chord.

The image shown in Fig. 13(e) (M_1 = 0.75 and $\Delta\beta_1 = -0.4^\circ$) is similar to that of Fig. 13(c) except for the additional leading edge shocks which do not appear to separate the boundary layer. However from Figs. 6 and 7, substantial differences in the surface Mach number distributions are apparent with an early separation of the turbulent boundary layer near 60-percent chord for the conditions in Fig. 13(e) and no apparent separation for the conditions in Fig. 13(c). This is confirmed by the losses; ω = 0.040 (Fig. 13(c)) and 0.086 (Fig. 13(e)).

V. Experimental and Computed Surface Mach Number Distributions

The surface Mach number distribution from the BGK two-dimensional code is compared to the experimental distribution for the near-design air angle and design Mach number in Fig. 6. The observed suction surface Mach numbers are lower than the design values in the supercritical region and higher over much of the downstream suction surface. This departure from the design distribution is not surprising in view of the observed premature laminar separation described previously. This laminar boundary layer separation conceivably produced a thick turbulent boundary layer which appeared to separate near the 60 percent chord point.

The OSONIC inviscid analysis code was used to predict the surface Mach number distribution at the off-design condition of minimum loss. The calculations were performed by assuming that laminar separation occurred at the 10-percent chord point. The airfoil shape was adjusted to account for the displacement thickness associated with the turbulent boundary layer which developed downstream of the assumed laminar separation point. The AVDR effect was also included in the analysis. The agreement in the overall shape between the calculated and experimental distributions is good as shown in Fig. 7. In this case the experimental and predicted distributions do not indicate turbulent boundary separation. As stated earlier, the loss coefficient for this case was less than half the value for the near-design case described above.

VII. Concluding Remarks

The results of this study indicate that it is difficult to experimentally establish transition on an airfoil having a "flat-roof-top" supersonic Mach number distribution as shown in Fig. 1. The satisfactory performance of such an airfoil depends critically upon the transitional behavior of the boundary layer which, in turn, depends on several factors such as Reynolds number, surface roughness, turbulence intensity, and AVDR. Surface roughness and turbulence intensity are not considered in the boundary layer prediction method by McNally[6] used herein. The results of this study suggest that a compatibility of experiment and theory might be realized if the transition point can be established with certainty. From a practical standpoint, this might be achieved by designing the airfoils with an accelerating Mach number distribution in the supercritical region similar to the distributions shown in Fig. 7 where the best performance was obtained.

A similar conclusion can be drawn from the supercritical airfoil experiments of Stephens[1] and Rechter et.al.[2] which were both performed in the DFVLR cascade. The results of Stephens show a theoretical design surface Mach number distribution which is very similar to the present one shown in Fig. 1 (BGK). Yet there was no evidence of a separation bubble near the leading edge and loss levels were low (ω = 0.02). It is conceivable that the results of Stephens differed so much from the present results because his observed surface Mach number distribution did not match the theoretical distribution in the leading edge region. Stephens attributed this to variations in the blade geometry as manufactured. The airfoils used in the present study were fabricated with a close tolerance and consequently were geometrically nearly perfect in the leading edge region.

In the Rechter et.al.[2] experiments the minimum total pressure loss coefficient at design conditions was about 0.05 for the flat-roof-top design (similar to the level measured in the present study). By altering the design surface Mach number distribution to permit acceleration over most of the supercritical region, the losses were reduced to about half the values obtained with the original design.

APPENDIX
Determination of Inlet Air Angle and Mach Number

The inlet air angle was determined from a combination of potential flow theory and the measurements from null-type probes located at the same relative tangential locations for three consecutive blade gaps. The potential flow calculations were performed at $\Delta\beta_1 = 0.0^\circ$ and $\pm 2.0^\circ$ to provide a map of inlet air angle as shown typically in Fig. 14 for the design condition. Each probe provided the flow angle at a point along the arc generated by the tip as it was rotated to attain a balance in pressure (null condition). By choosing the tangential location of each probe relative to the blade gap as shown in Fig. 14, the arc in which the local angle was measured passes through a region in which flow angle variations are small. A plot of the difference between the indicated and theoretical flow angles as a function of indicated flow angle was established for each value of $\Delta\beta_1$. The indicated flow angles corresponding to a zero difference between the indicated and theoretical flows along the arc of measurement were then crossplotted to yield a linear variation of the actual flow angle one chord length upstream of the cascade as a function of indicated angle from the probe.

Similar potential flow calculations indicated that the inlet Mach number one chord length upstream of the cascade could be obtained from the ratio of the average value of static pressure from

five equally spaced pressure taps across the center passage to the total pressure. The five static pressure taps were located 0.13 C upstream of the blade row as shown in Fig. 14. The inlet Mach number was computed as a function of this pressure ratio using the isentropic flow relationships for a perfect gas.

VIII. References

1. Stephens, H. E., "Application of Supercritical Airfoil Technology to Compressor Cascades: Comparison of Theoretical and Experimental Results," AIAA Paper 78-1138, July 1978.
2. Rechter, H., Schimming, P., and Starken,H., "Design and Testing of Two Supercritical Compressor Cascades," ASME Paper 79-GT-11, Mar. 1979.
3. Boldman, D. R., Buggele, A. E., and Michalson, G. M., "Stall Flutter Experiment in a Transonic Oscillating Linear Cascade," NASA TM-82655, Nov. 1981.
4. Bauer, F., Garabedian, P., and Korn, D., Supercritical Wing Sections, Vol. I, II, and III, Springer-Verlag, New York, 1972, 1975, 1977.
5. Sanz, J. M., "Design of Supercritical Cascades with High Solidity," AIAA Paper 82-0954, June 1982.
6. McNally, W. D., "Fortran Program for Calculating Compressible Laminar and Turbulent Boundary Layers in Arbitrary Pressure Gradients," NASA TN D-5681, May 1970.
7. Nash, J. F., and MacDonald, A. G. J., "The Calculation of Momentum Thickness in a Turbulent Boundary Layer at Mach Numbers up to Unity," Aeronautical Research Council, ARC-CP-963, 1967.
8. Preston, J. H., "The Minimum Reynolds Number for a Turbulent Boundary Layer and the Selection of a Transition Device," Journal of Fluid Mechanics, Vol. 3, Pt. 4, Jan. 1958, pp. 373-384.
9. Stratford, B. S., "The Prediction of Separation of the Turbulent Boundary Layer," Journal of Fluid Mechanics, Vol. 5, Pt. 1, Jan. 1959, pp. 1-16.
10. Farrell, C. A., "Computer Program for Calculating Full Potential Transonic, Quasi-Three-Dimensional Flow Through a Rotating Turbomachinery Blade Row," NASA TP-2030, June, 1982.
11. Peacock, R. E., "Flow Control in the Corners of Cascades," Aeronautical Research Council Report, ARC-27291. Oct. 1967.
12. Stark, U., and Hoheisel, H., "The Combined Effect of Axial Velocity Density Ratio and Aspect Ratio on Compressor Cascade Performance," ASME Paper 80-GT-138, Mar. 1980.
13. Starken, H., Breugelmans, F. A. E., and Schimming, P., "Investigation of the Axial Velocity Density Ratio in a High Turning Cascade," ASME Paper 75-GT-25, Mar., 1975.
14. Starke, J., "The Effect of the Axial Velocity Density Ratio on the Aerodynamic Coefficients of Compressor Cascades," ASME paper 80-GT-134, Mar. 1980.

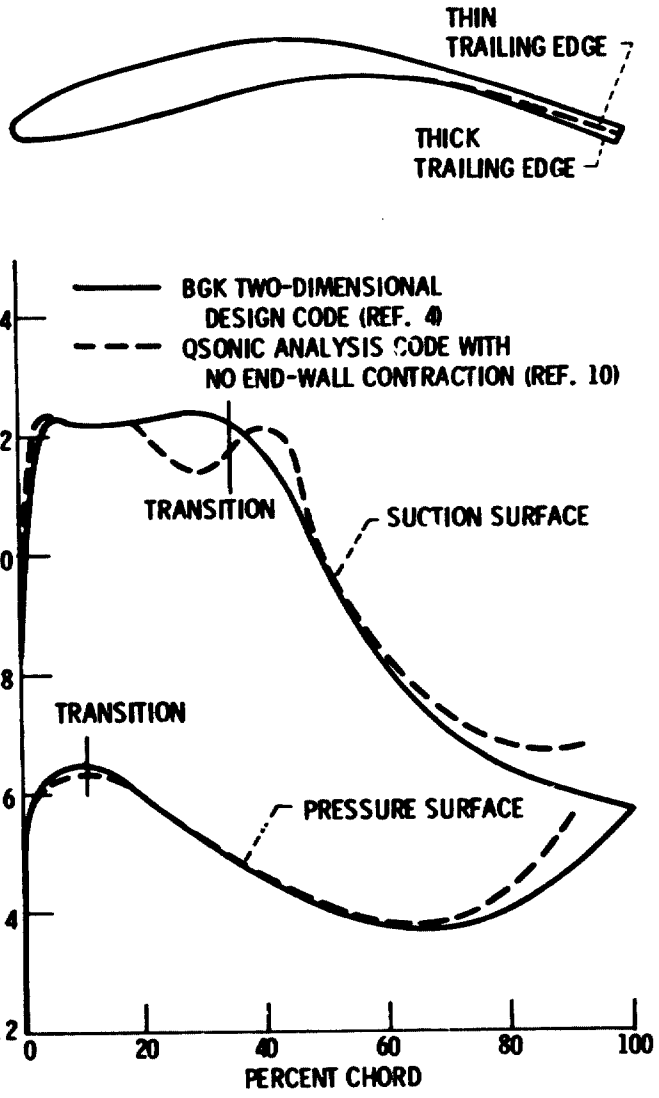

Figure 1. - Surface Mach number distributions for the thick-trailing-edge airfoil based on design and analysis codes, $M_1 = 0.754$, $M_2 = 0.560$, $C/\tau = 0.91$, $\Delta\beta_1 = 0^\circ$.

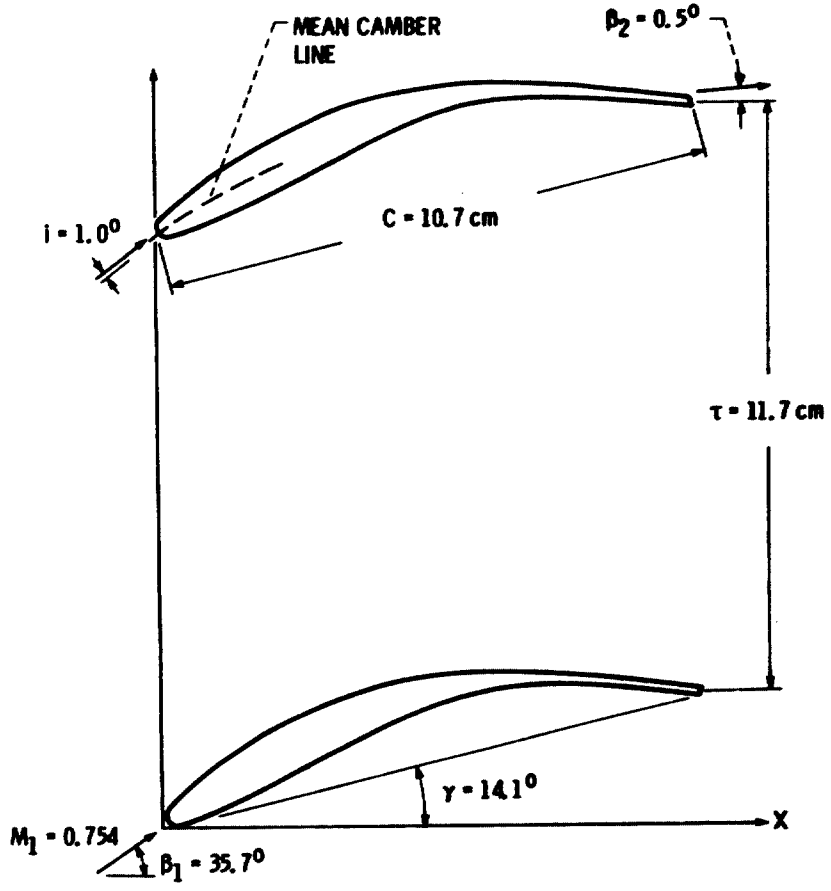

Figure 2. - Design conditions and coordinate system.

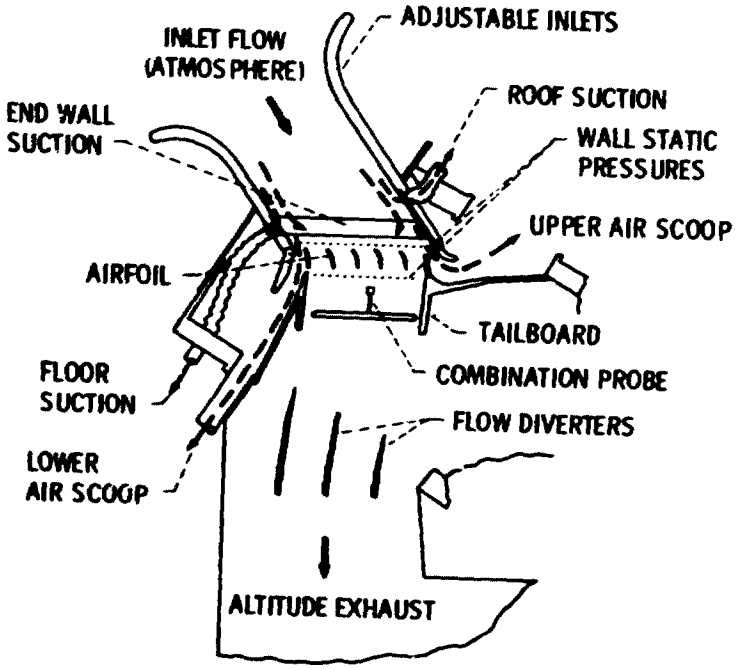

Figure 3. - Schematic diagram of transonic cascade facility.

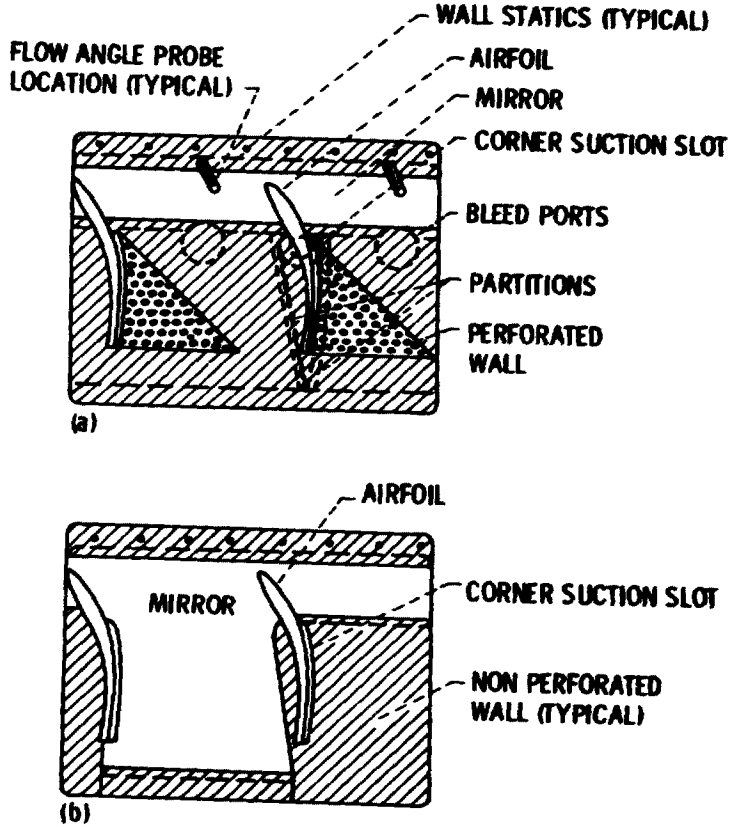

(a) Passage and slot bleed configuration.
(b) Slot bleed and schlieren mirror configuration.

Figure 4. - Center blade passage details.

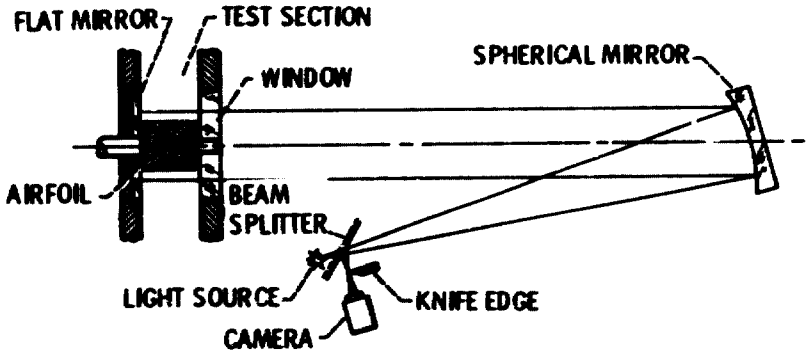

Figure 5. - Double-pass schlieren system.

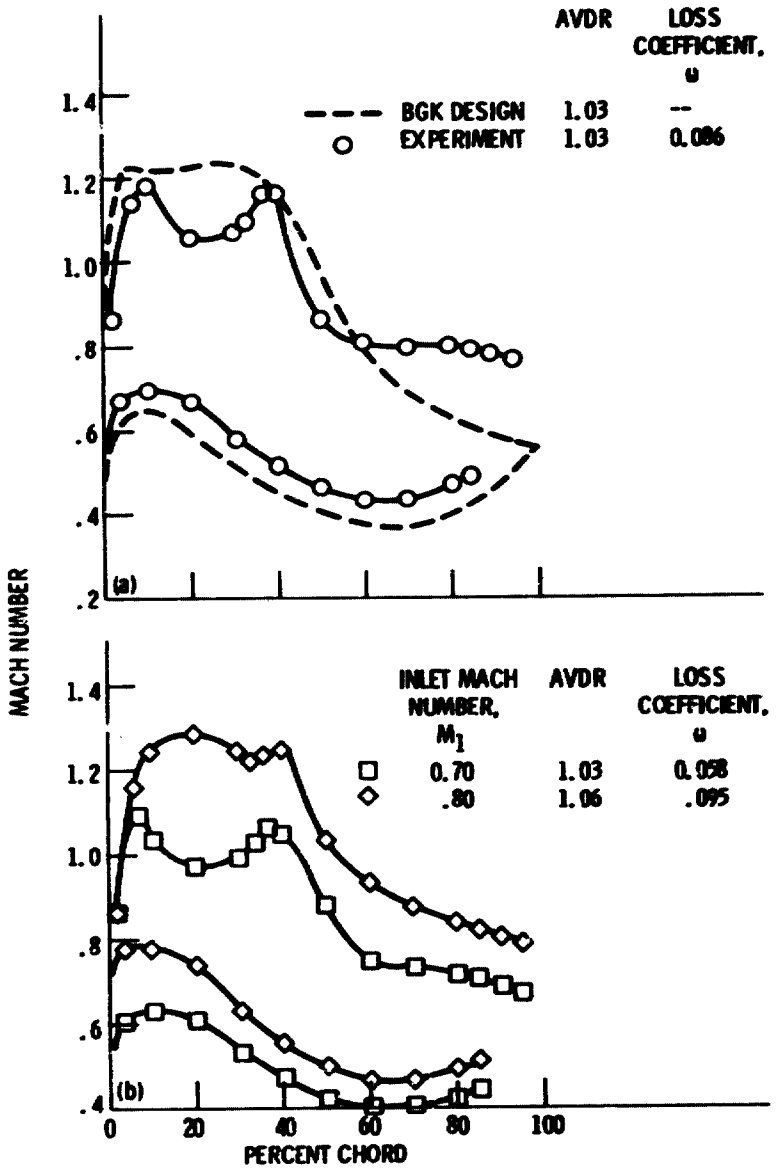

(a) M_1 = 0.75 (DESIGN).
(b) M_1 = 0.70 and 0.80.

Figure 6. - Surface Mach number distributions for thin-trailing-edge airfoil near the design inlet air angle, $\Delta\beta_1 = -0.4^\circ$.

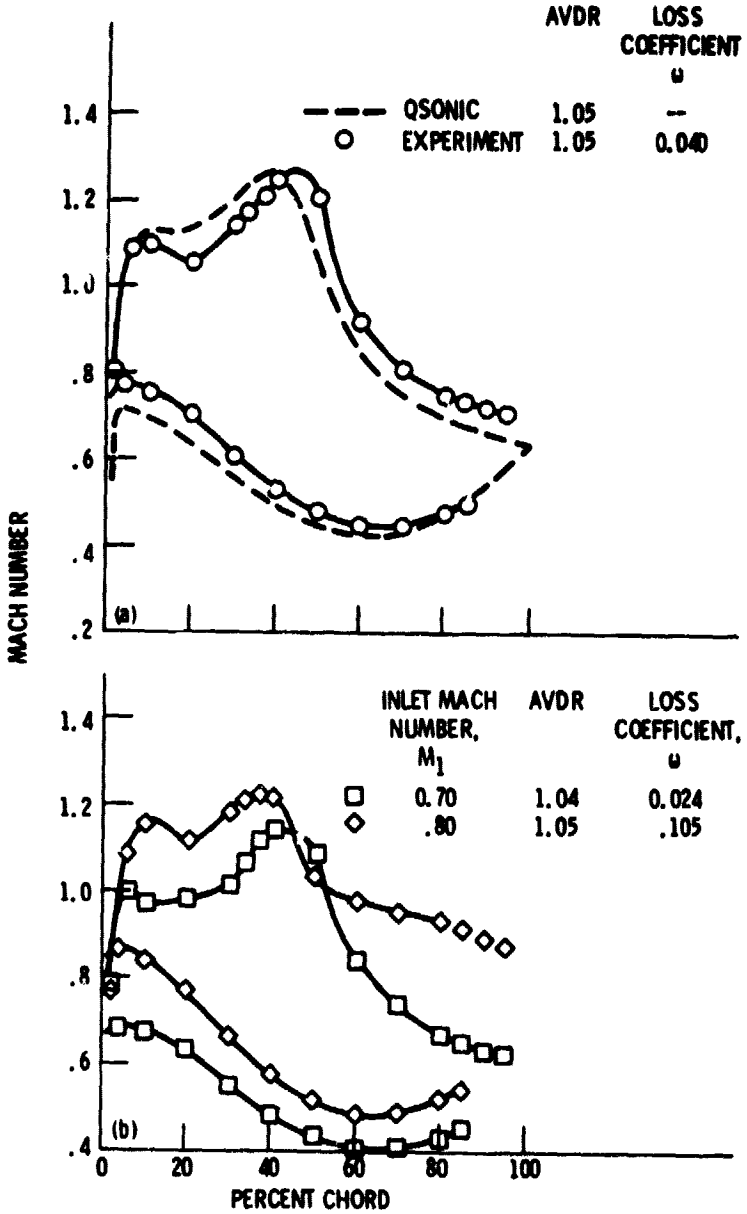

(a) M_1 = 0.75 (DESIGN).
(b) M_1 = 0.70 and 0.80.

Figure 7. - Surface Mach number distributions for thin-trailing-edge airfoil at minimum-loss inlet air angle, $\Delta\beta_1 = -2.5^0$.

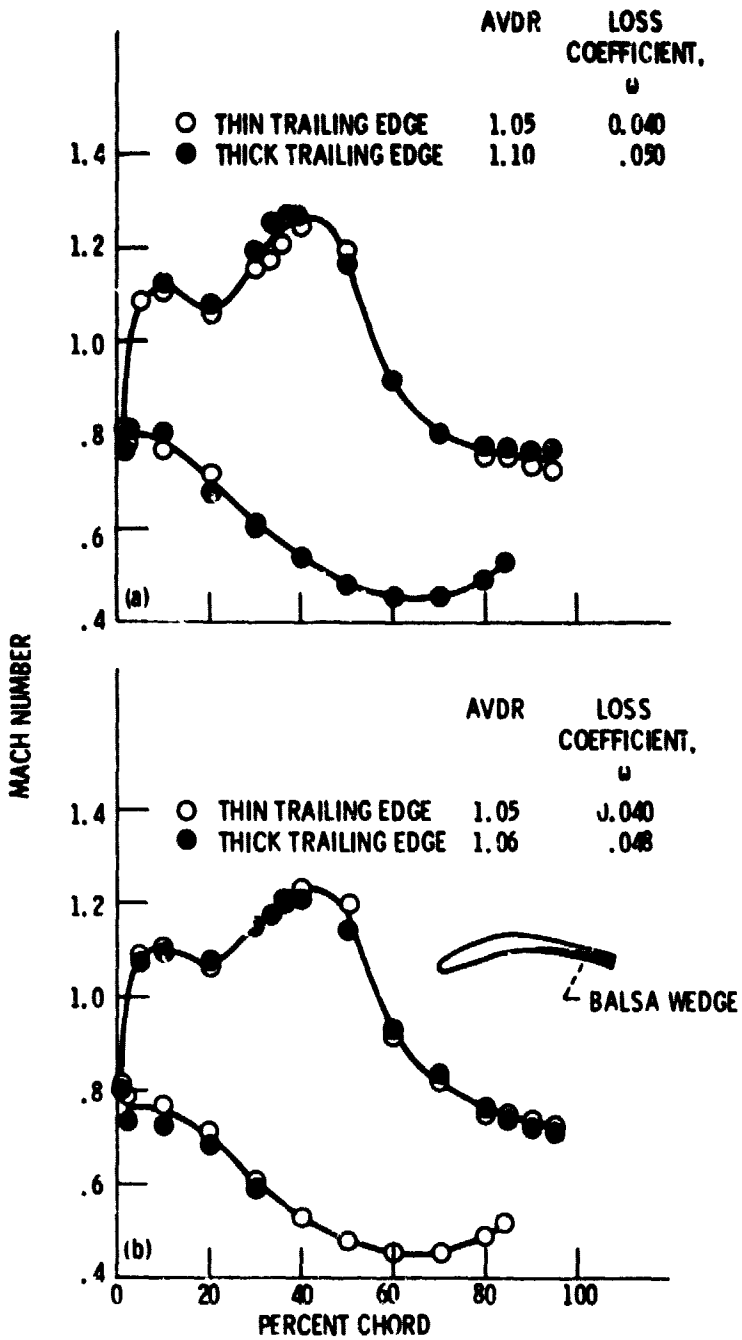

(a) Thick trailing edge as machined.

(b) Thick trailing edge formed by addition of balsa wedge to pressure surface of machined thin-trailing-edge airfoil.

Figure 8. - Comparison of surface Mach number distributions for thick- and thin-trailing-edge airfoils at design inlet Mach number, $M_1 = 0.75$ and at minimum-loss inlet air angle, $\Delta\beta_1 = -2.5^0$.

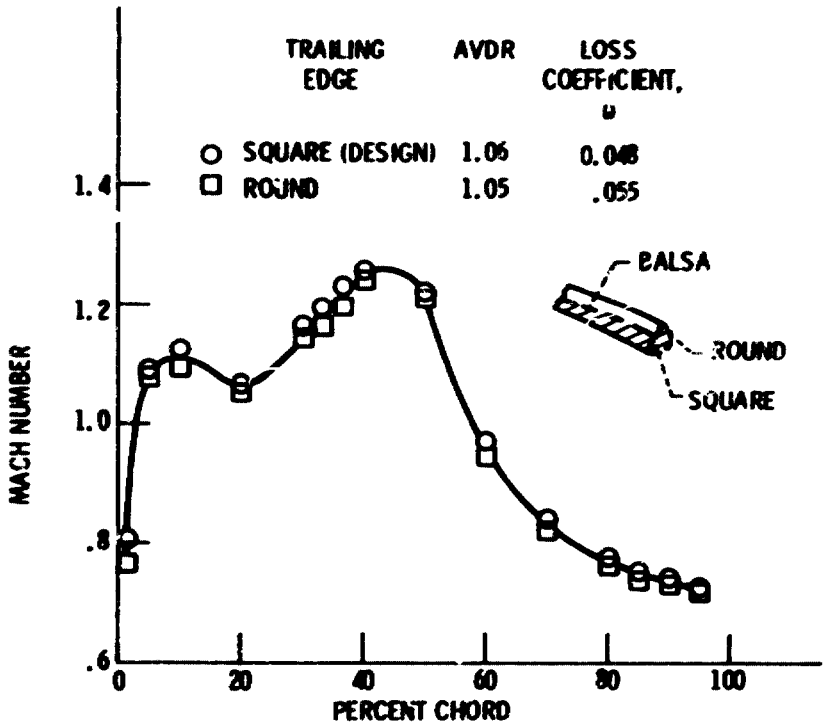

Figure 9. - Suction-surface Mach number distribution for airfoils with square and round thick trailing edges. $\Delta\beta_1 = -2.5^0$; $M_1 = 0.75$.

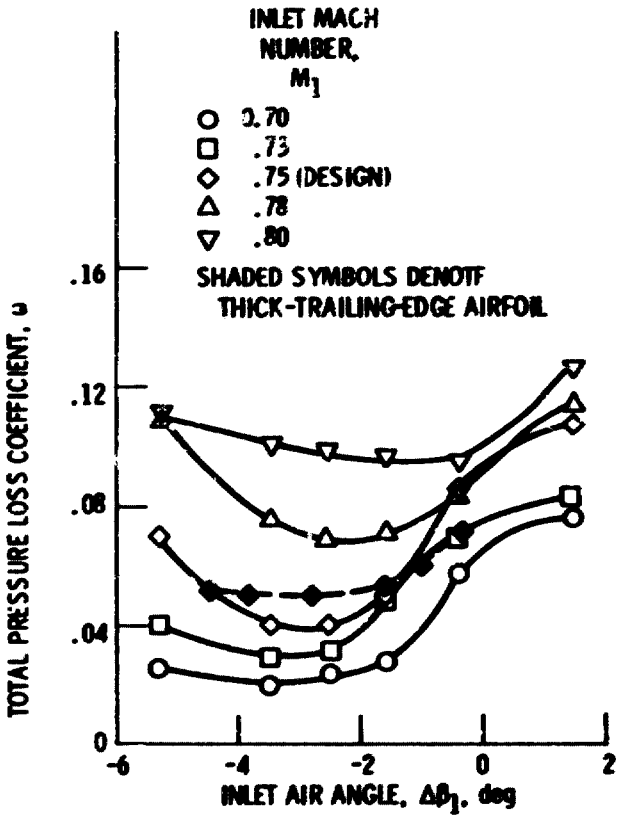

Figure 10. - Variation of total pressure loss coefficient with inlet air angle for thin-trailing-edge airfoil.

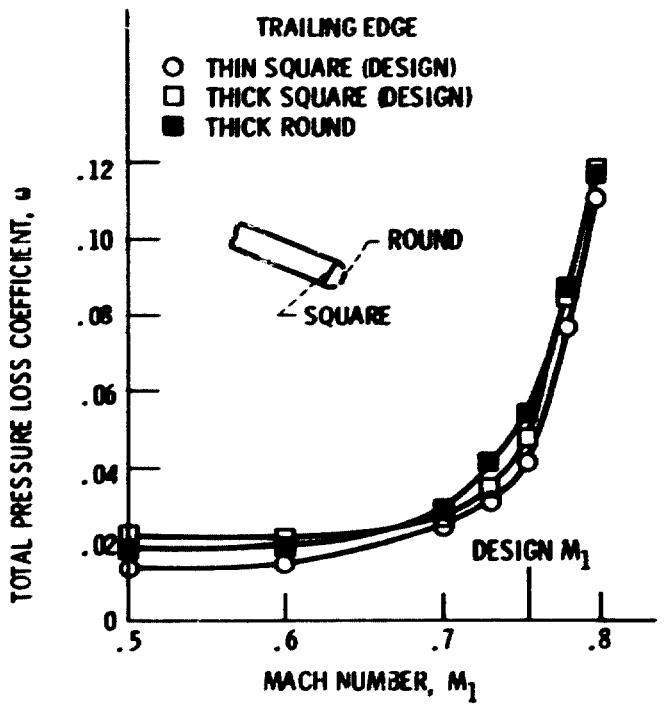

Figure 11. - Variation of total pressure loss coefficient with trailing-edge thickness and shape at minimum-loss inlet air angle. $\Delta\beta_1 = -2.5^0$.

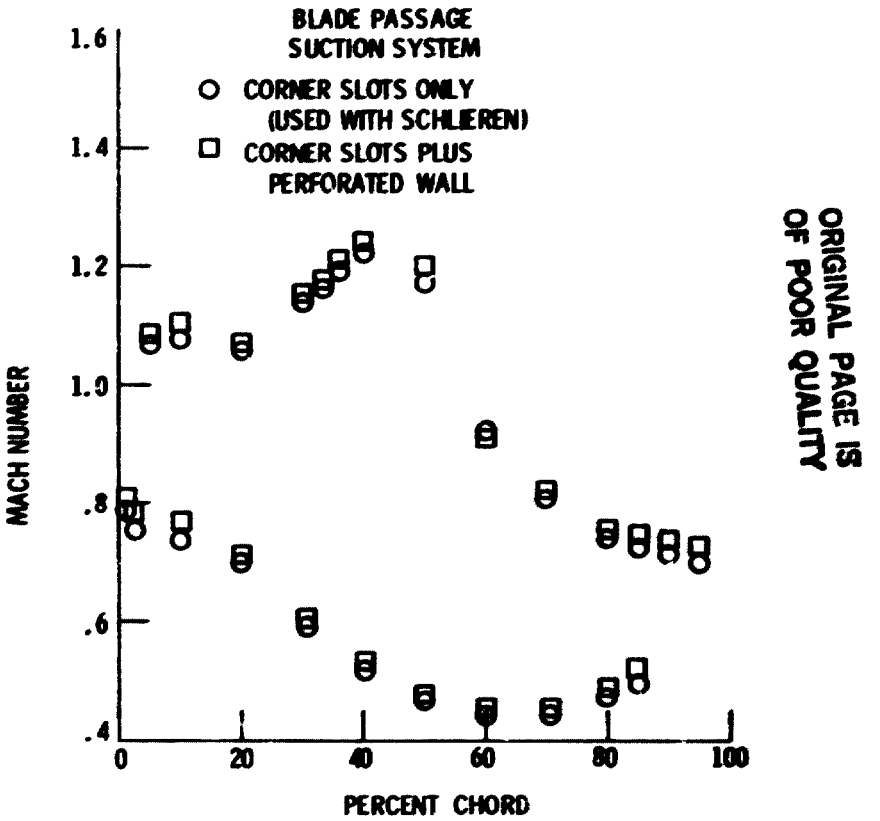

Figure 12. - Comparison of surface Mach number distributions with different end-wall suction systems. $\Delta\beta_1 = -2.5^0$ $M_1 = 0.75$.

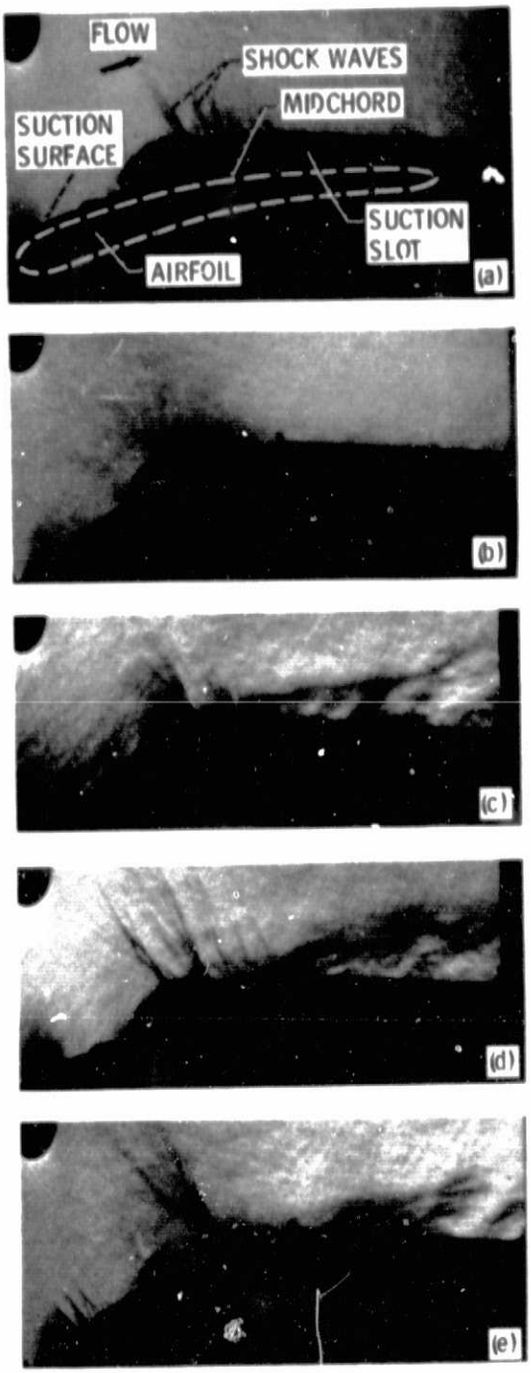

(a) $\Delta\beta_1 = -2.5^0$; $M_1 = 0.70$; $\omega = 0.024$.
(b) $\Delta\beta_1 = -2.5^0$; $M_1 = 0.73$; $\omega = 0.032$.
(c) $\Delta\beta_1 = -2.5^0$; $M_1 = 0.75$; $\omega = 0.040$.
(d) $\Delta\beta_1 = -2.5^0$; $M_1 = 0.80$; $\omega = 0.100$.
(e) $\Delta\beta_1 = -0.4^0$; $M_1 = 0.75$; $\omega = 0.086$.

Figure 13. - Schlieren images of flow over one airfoil in cascade.

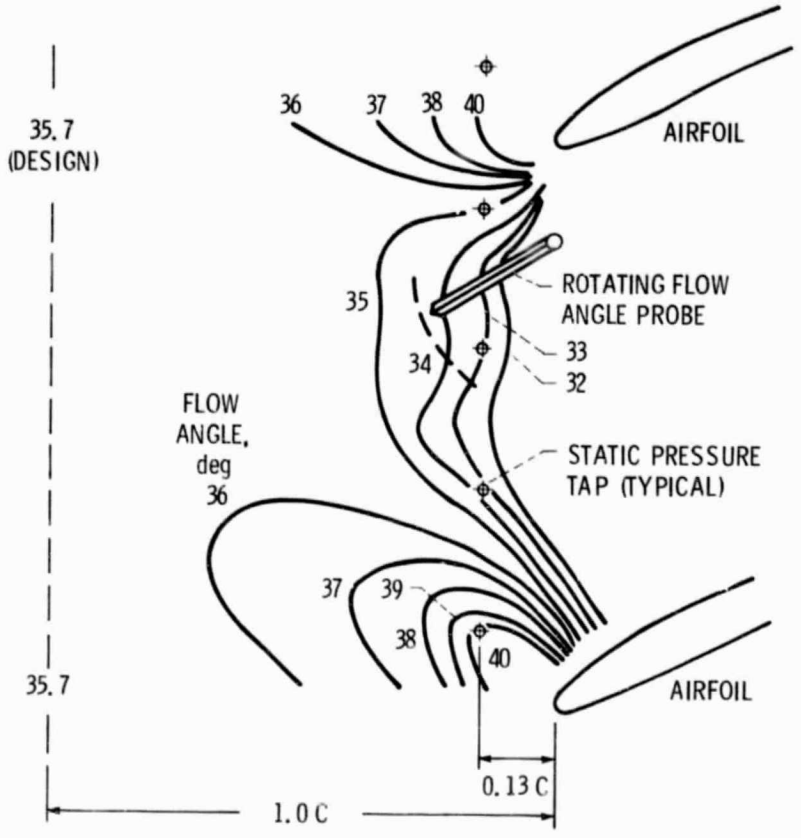

Figure 14. - Design air angle contours based on QSONIC (ref. 10).